An Adaptable Blueprint for Non-Metal Near-Infrared Organic Photocatalysts by Aromatic Sulfones

Kazuya Yoshida[a], Toshiaki Suzuki[b], Vasudevanpillai Biju*[a,c], Yuta Takano*[a,c]

[a]*Graduate School of Environmental Science, Hokkaido University, N10, W5, Sapporo 060-0810, Japan.*

[b]*Unisoku Co. Ltd, Hirakata, Osaka 573-0131, Japan.*

[c]*Research Institute for Electronic Science, Hokkaido University, N20, W10, Sapporo 001-0020, Japan.*

.

KEYWORDS. Photoredox catalysts, electron transfer reactions, radical reactions, sulfone-rosamine, NIR dye molecules

ABSTRACT: We present a versatile approach to designing and utilizing high-performance non-metal near-infrared (NIR) organic photocatalysts based on aromatic sulfones. Current NIR photocatalysts are mainly metal complexes and inorganic materials, while the few reported non-metal organic NIR photocatalysts primarily use photosensitization to produce active species such as singlet oxygen. Our sulfone-rosamine-based redox photocatalyst **3** demonstrates exceptional capabilities, including high ability for metal-free photo-oxidative bromination, intrinsically oxygen-independent redox reactions, and remarkable photostability with a turnover number (TON) exceeding 2800. We showcase the photocatalyst's efficacy in photo-oxidative bromination of aromatic compounds under 738 nm illumination. The reaction mechanism is elucidated through electrochemical studies, time-resolved spectral measurements, and DFT calculations. Transient absorption measurements using the randomly interleaved pulse train (RIPT) method reveal the photo-excited state of **3** in the reaction. The photocatalyst **3** demonstrated its versatility for several aromatic substances, including those exhibiting strong light absorption in the visible region. This aromatic sulfone-based approach offers a robust blueprint for developing non-metal NIR organic photocatalysts with superior photo-oxidation ability and stability, addressing key limitations of conventional organic NIR photocatalysts.

Introduction

Photoredox catalysis has revolutionized covalent bond formation under mild conditions.[1] Non-metal organic catalysts offer advantages in cost-effectiveness and low environmental impact.[2] However, most organic photocatalysts primarily use UV-visible light, which presents challenges such as selectivity issues, undesirable side reactions, and competition with substrates and products for light absorption.[1,3]

The expansion of organic photocatalysts into the near-infrared (NIR) region (≧ 700 nm) has gained significant interest.[3] NIR light's high permeability allows for broader applications based on more extensive substrate selection and fewer side reactions in photocatalytic processes.[4,5]

Despite their potential, the development of NIR organic photocatalysts has faced challenges. The main reason is that limited organic molecules can efficiently absorb NIR light energy and utilize it for catalytic reactions. This limitation stems from the difficulty in designing organic structures that combine a narrow band gap and high reactivity in the photoexcited state. Current NIR photocatalysts are predominantly metal complexes,[3,6] upconverting organic molecules[7] or inorganic materials.[8]

Among the scarce non-metal organic NIR photocatalysts, molecules such as squaraine[9] and cyanine dyes[10] have shown promise, primarily utilizing photosensitization to generate active reaction intermediates like singlet oxygen.[11] However, this mechanism constrains oxidizing power and the choice of substrates. Moreover, singlet oxygen may degrade the photocatalysts, lowering their photo-stability indicated by small turnover numbers (TON). Indeed, TONs were rarely reported for NIR organic photocatalysts (Table S1, see the supporting information), implying their low stability.

This study introduces a versatile strategy for designing non-metal organic photocatalytic molecules that employ a photoinduced electron transfer reaction triggered by NIR light. Our NIR photocatalyst **3** (Figure 1A), a xanthene dye with an SO_2 moiety, achieves an energetic state suitable for reductive quenching cycles of photoredox reactions (Figure 1B), showing the highest photo-oxidation ability (E_{red1}*: 1.35 V vs. Fc/Fc^+) and TON (2830) among single molecular NIR photocatalysts.

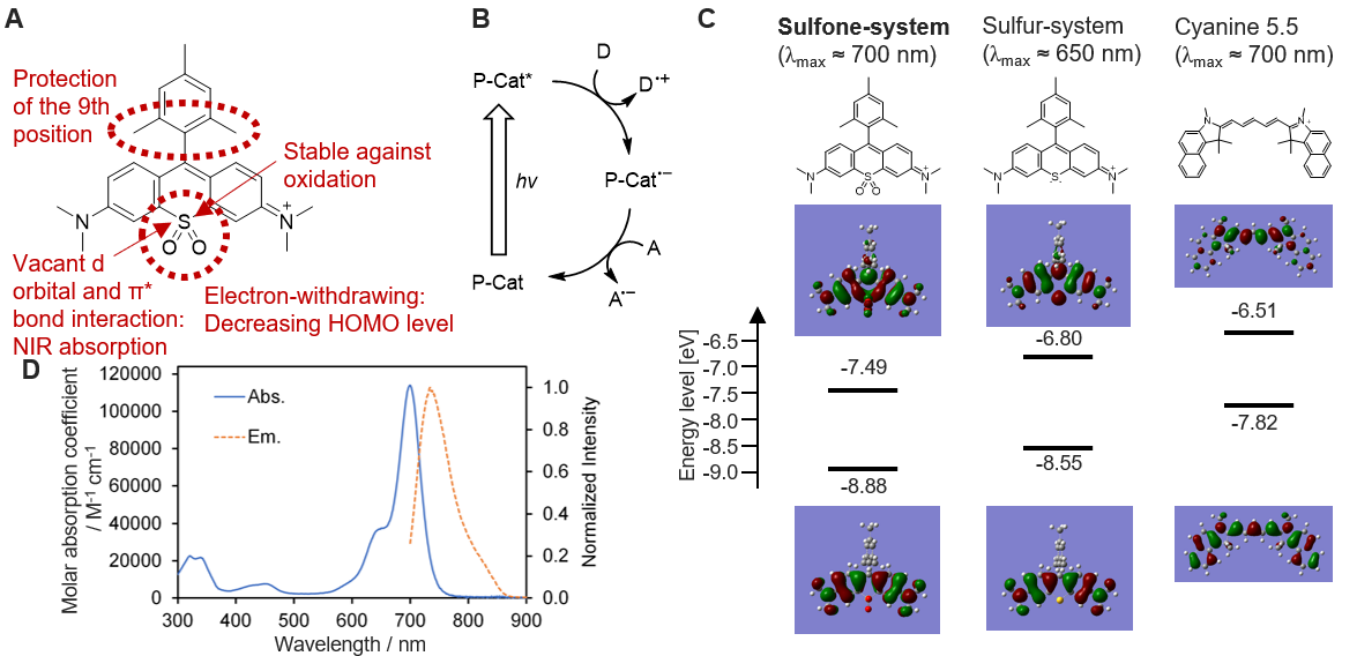

Figure 1. (A) The molecular structure of sulfone-rosamine **3**, where the counter anion CF_3COO^- is omitted for clarity, (B) reductive quenching cycles of a photoredox catalyst, where P-Cat: photocatalysts, D: electron donor, A: electron acceptor, (C) HOMOs and LUMOs of the present sulfone-system (left) and a corresponding sulfur system (center) and a cyanine 5.5 (right) as comparisons, obtained by DFT calculations at the LSDA/6-311+G** level along with reported values of λ_{max},[19,22] and (D) absorption and fluorescence spectra (WL_{ex}: 690 nm) of **3** in MeCN.

We focus on aromatic sulfones as a promising class of compounds for developing adaptable non-metal organic NIR photocatalysts (Figure 1A). Combining the advantages of organic non-metal photocatalysts with NIR light benefits represents a significant advancement in photoredox catalysis. Our molecular design strategy opens new avenues for sustainable technologies and expands the possibilities in the field.

EXPERIMENTAL

General information

A UV-Vis spectrophotometer (Evolution 220, Thermo Fisher Scientific, USA) and a fluorescence spectrophotometer (RF-6000, Shimadzu Co., Japan) were used to record the absorption and fluorescence spectra. ^1H and ^{13}C NMR spectra were measured using a JEOL JNN-EX400 spectrometer (Tokyo, Japan). Electrospray ionization (ESI)mass spectra were recorded using a JEOL JMS-T100LC instrument (Japan).

All chemicals used in this study were of analytical grade and were used as received unless otherwise stated. Reagent-grade solvents were obtained from FUJIFILM Wako Pure Chemical Corporation (Osaka, Japan).

Density functional theory (DFT) calculations

The geometries of the molecules were optimized using the Gaussian 16 Revision C.01 program with the Local Spin Density Approximation (LSDA) functional in the default Gaussian 16 package[12]. The LSDA is a method keyword in Gaussian 16 that requires a local spin density approximation calculation using the Slater exchange functional and VWN correlation functional for the DFT calculation. The 6-311+G(d,p)[13–15] basis set was used. Molecular orbital analyses were performed with the natural transition orbitals (NTO).[16]

Transient absorption spectral measurements

Subnanosecond laser-induced transient absorption spectra were collected by a commercially available measuring system (picoTAS; Unisoku, Japan) based on the randomly interleaved pulse train (RIPT) method developed by Nakagawa et al.[17] The pump source is a mode-locked picosecond laser (PL2210A/PG403, EKSPLA, 1 kHz, 25 ps, 355 nm/410-2300 nm). The time resolution of the system was estimated to be 100 ps from a 10 to 90% rise time. For nanosecond laser flash photolysis experiments, deaerated MeCN solutions of the sample were excited by a Nd:YAG laser (Continuum, SLII-10, 4–6 ns FWHM) at 355 nm with a power of 10 mJ per pulse. Transient absorption measurements in the visible and near-IR regions were performed with a continuous xenon lamp (75 W) as the probe light, a photomultiplier (Hamamatsu R2949; 350–800 nm), and an InGaAs PIN photodiode (Hamamatsu G10899-01K; 800–1600 nm) as the detector. The outputs from the photodiodes and photomultiplier were recorded using a digitizing oscilloscope (HDO4022, Teledyne Lecroy, 200 MHz).

Electrochemical Measurements:

Electrochemical measurements were performed using a BAS ALS 630 electrochemical analyzer. The redox potentials were determined by differential pulse voltammetry (DPV) in dried and argon-purged MeCN. A glassy carbon (3 mm diameter) working electrode, $Ag/AgNO_3$ reference electrode, and Pt wire counter electrode were used. Ferrocenium hexafluorophosphate was used as the internal standard.

Photocatalytic reactions by 3

Typically, a CD_3CN solution (0.75 mL) containing **3** (0.2 mM), a substrate (4.0 mM), and HBr aq. (20 mM), in a quartz cuvette with a silicon lid. Dimethylsulfone (DMS, 0.08 mM) was added as an internal standard. The solution was irradiated with an LED (738 ± 34 nm, 370 mW / cm^2). After photoirradiation, the corresponding brominated product was identified and quantified by comparing the ^1H NMR spectra with an authentic sample and the internal standard.

Photocatalytic bromination by 3 in the absence of O_2

The CD_3CN solvent (0.75 mL) in a sealed test tube was added with **3** (0.2 mM), TMB (4.0 mM), and HBr aq. (20 mM), and freeze-pump-thaw cycling was repeated three times, and argon was added. The solution was irradiated with an LED (738 ± 34 nm, 370 mW/cm^2) and stirred. The reaction solution was analyzed using ^1H NMR spectroscopy and absorption spectra.

RESULTS AND DISCUSSION

Molecular designing strategy, synthesis, and characterization

We designed sulfone-rosamine with a mesityl group (**3**) as a candidate for an NIR photocatalytic molecule, supported by theoretical calculations (Figures 1A and 1C). Although sulfone-rosamines have been previously studied for their unique NIR absorption and fluorescent properties,[18–20] their photocatalytic ability remains unexplored. We hypothesized that sulfone-rosamines could act as excellent photooxidants because of their remarkably lower HOMO levels compared to other NIR dyes such as sulfur-rhodamines and cyanines (Figure 1C). The strong electron-withdrawing nature of the SO_2 moiety decreases the electron density of the aromatic system,[21] resulting in a low HOMO level, which is crucial for photoinduced oxidative electron transfer reactions as the initial step of photocatalytic reactions (Figure 1B).

The use of aromatic sulfones offers two additional advantages as photocatalysts. First, it enhances photo-stability. The attachment of two oxygen atoms to the sulfur atom significantly lowers the corresponding triplet excited state, decreasing the probability of intersystem crossing from its singlet excited state. DFT calculations suggest a remarkably low triplet excited level in **3**, where intersystem crossing is unlikely to occur (Figures S1 and S2, see Supporting Information). While B3LYP is often the first choice for DFT calculations, it tends to overestimate the first transition energy corresponding to the first absorption maximum for aromatic sulfones.[22] Thus, the LSDA was used in the present study because it demonstrated the best match with the experimentally observed values (Table S2). This property prevents singlet oxygen generation, which can degrade compounds in photoredox reactions. This was experimentally confirmed using 1,3-diphenylisobenzofuran (DPBF) as a chemical probe for singlet oxygen detection. The corresponding absorption spectra and absorption time-time profiles of the reaction mixture are shown in Figure S3, indicating extremely low singlet oxygen production efficiency of **3** compared to that of Rose Bengal (QY: 53 %[23]). Conversely, singlet oxygen production by **3** is negligibly small.

Second, the use of aromatic sulfones provides chemical stability. The SO_2 moiety decreases the electron density of the molecules, resulting in resistance to oxidation. Consequently, aromatic sulfone compounds are generally stable against oxidative decomposition, making them suitable photoredox catalysts. Moreover, sulfone-rosamines possess a small HOMO-LUMO gap originating from a interaction between the vacant d-orbital on the sulfur atom and the π^* bond,[18] enabling NIR light absorption(Figure S4).

The synthesis of target molecule **3** involved a two-step process (Schemes S1 and S2). Initially, a sulfonation reaction using bis[4-(dimethylamino)phenyl]methane as the starting material afforded 3,6-bis(dimethylamino)-9H-thioxanthen-9-one-10,10-dioxide (**2**). Subsequently, an organolithium reaction using **2** yielded the target product, 9-mesityl sulfone-rosamine with trifluoromethylacetate (CF_3COO^-) as the counter anion (**3**). Introducing the mesityl group at the 9-position is crucial to protect this position from undesired nucleophilic attack.[24] Measurements, including absorption, fluorescence, high-resolution ESI mass spectra, and NMR spectra, confirmed the successful formation and isolation of product **3** (Figures S5 and S6).

The absorption spectrum of **3** exhibits a characteristic NIR absorption band at 700 nm in MeCN (Figure 1D), with a molar absorption coefficient of 1.14×10^5 M^{-1} cm^{-1}. This result indicates that **3** can effectively utilize NIR light over 700 nm. Additionally, **3** demonstrated moderate fluorescence centered at 734 nm with a quantum yield (Φ_{FL}) of 0.160 (Figure 1D), implying an efficient formation of the singlet excited state.

Photophysical properties and redox potentials

The transients of **3** were observed and explained through sub-nanosecond transient absorption (sns-TA) spectral and time-resolved fluorescence spectral measurements and were supported by DFT calculations. We employed the randomly interleaved pulse train (RIPT) method,[17] which can cancel emission signals and enables clear observation of transient absorption spectra on the time scale where emission exists simultaneously, that is typically 1-100 ns for organic molecules.

sns-TA spectra of **3** in argon-purged MeCN demonstrated remarkable bleach signals centered at 700 nm with a rate constant of 4.3×10^8 (τ: 2.3 ns) by single exponential fitting (Figures 2A and 2B). This was accompanied by signals at 500 nm and 640 nm, exhibiting identical rate constants to 700 nm, indicating their common origin in the excited state.

The time-resolved fluorescence decays of **3** demonstrated a single exponential decay with a lifetime of 2.4 ns (Figure 2C). Considering the intrinsic errors of the apparatuses (< 5% error), this result indicates that the observed decay at 700 nm in sns-TA spectra (τ: 2.3 ns) is attributed to the first singlet excited state of **3**. The comparable lifetimes suggest negligible nonradiative recombination from the singlet excited state.

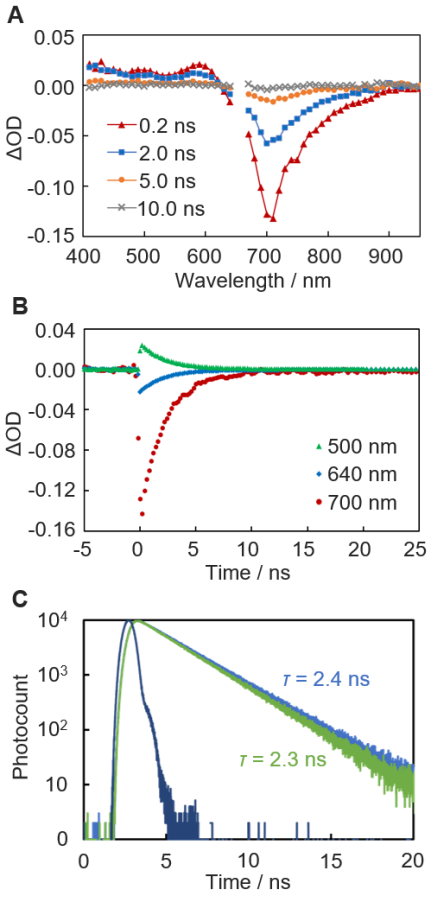

Figure 2. (A) Transient absorption spectra of **3** (WL_{ex}: 660 nm), (B) decay profiles obtained from Figure 2A, and (C) time-resolved fluorescence decays of **3** (WL_{ex}: 630 nm, WL_{em}: 725 nm) in the presence (green) and absence (blue) of 20 mM HBr and the instrumental response function (IRF) (dark blue). Solvent: MeCN.

Another important observation from the sns-TA spectra is the absence of a detectable triplet excited state for **3**. We measured the spectra up to 1600 nm and could not detect any signals other than its singlet excited state (Figure S7). Natural transition orbital (NTO) analysis by DFT calculations predicted a low probability of triplet excited state formation (Figure S1B). The efficiency of intersystem crossing can be predicted by the energy gap between the singlet and triplet excited states,[25] in which a smaller gap corresponds to a larger probability of the intersystem crossing. In **3**, this gap is 0.87 eV, which is much larger than the corresponding sulfur-rosamine (0.33 eV) or other compounds showing characteristic triplet signals in TA.[26] Consequently, **3** was found to be an excellent molecule for utilizing its singlet excited state energy in photocatalytic reactions while avoiding side effects caused by the triplet excited state and singlet oxygen generated by energy transfer from the triplet state.[26]

Redox potential measurements were performed to characterize the photocatalyst **3** further. Table 1 shows the data for **3** and 9-mesityl acridinium (Mes-Acr$^+$) dyad, one of the most studied photoredox catalysts invented by Fukuzumi and co-workers.[1,27,28] It was found that **3** possesses a first reduction potential of 1.35 V vs. Fc/Fc$^+$ couple in its photo-excited state (E_{red1}*).[1] To our knowledge, this value is the highest among the reported organic NIR-photocatalysts (cf. an osmium-cased complex, **Os16**[4]; E_{red1}*: 1.14 V vs. Fc/Fc$^+$, by subtracting +0.10 V from the reported value in V vs. Ag/AgCl), suggesting that **3** could act as a strong photo-oxidant in photocatalytic reactions.

As the photocatalytic reactions were performed in the presence of 10 mM HBr (vide infra), we also recorded the potentials of **3** in the presence of 10 mM HBr (Table 1). We found no remarkable change in the values, particularly in its reduction potentials (-0.42 V without HBr and -0.41 V with HBr). We also confirmed that the absorption, fluorescence, and TA spectra did not change after adding HBr (Figure S8). This stability in the presence of HBr further supports the potential of **3** as an effective photocatalyst under acidic reaction conditions.

Table 1. Redox potentials[a] and $E_{0,0}$ values[b]

	E_{red1} [V]	E_{ox1} [V]	$E_{0,0}$ [eV] [b]	E_{red1}* [V] [c]
3	-0.42	1.05[d]	1.75	1.33
3 in HBr	-0.41	0.95[d]	1.75	1.34
Mes-Acr$^+$	-0.95[e]	1.68[e]	2.57[e]	1.62

[a] Values versus Fc$^{0/+}$ couple. Conditions: A glassy carbon electrode was the working electrode, the counter electrode was the platinum wire, and Ag/Ag$^+$ was the reference electrode. [b] Obtained from the offset in the absorption spectra. [c] Obtained from E_{red1} + $E_{0,0}$ according to Ref[1]. [d] Irreversible. [e] Obtained from Ref[29], where the redox potentials vs. SCE were subtracted by +0.38 to set Fc$^{0/+}$ as the standard.

The thermodynamic feasibility of photocatalytic oxidative reactions was determined from the Gibbs free energy change ($\Delta G'$) of photoinduced electron transfer based on the the well-established Rehm-Weller equation[30]:

$$\Delta G' = E_{ox}(Sub.) - E_{red}(\mathbf{3}) - E_{0,0}(\mathbf{3}) \qquad \text{eq. 1}$$

where E_{ox}(Sub) is obtained from the first oxidation potential of the substrate of interest, E_{red}(**3**) is from the reduction potential of **3**, and $E_{0,0}$(**3**) is the zero-zero excitation energy of **3**. eq. 1 in the present case is equal to:

$$\Delta G' = E_{ox1}(Sub.) - E_{red1}*(\mathbf{3}) \qquad \text{eq. 2}$$

where E_{red1}*(**3**) is the estimated reduction potential of **3** in its photoexcited state.[1]

For instance, considering the photo-oxidation of 1,3,5-trimethoxybenzene (TMB) with an oxidation potential of 1.05 V, and applying the equation to this reaction using **3**,

$\Delta G'$ = 1.05 eV − (−0.42 eV) −1.75 eV = −0.28 eV = −4.5 × 10^{-20} J

The negative value of ΔG' (−0.28 eV= −4.5 × 10^{-20} J) indicates that the photo-oxidation is thermodynamically favorable.

Photocatalytic bromination by 3

To verify the utility of **3** as a NIR photoredox catalyst, we selected photocatalytic bromination for this study, as it is a

useful reaction for preparing various functional molecules and drugs. [27,31]

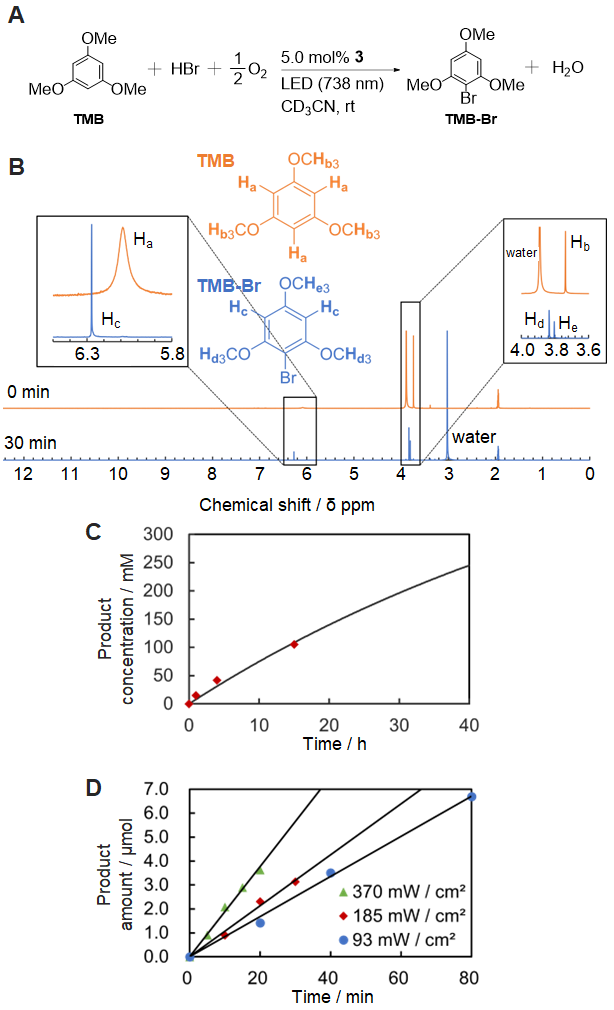

Figure 3. (A) The photocatalytic reaction scheme using TMB, HBr and **3**, (B) ^{1}H-NMR spectra of the reaction mixture before (orange, upper) and after (blue, lower) 30 min illumination of 738 nm light, (C) time profile of the generation of the brominated product, TMB-Br, using excess amount of TMB and HBr, with a fitting curve extrapolating production amount and (D) light-intensity-dependent generation of the brominated product. The peak position of water in ^{1}H-NMR spectra changed after the reaction because of the pH change.

Based on the redox potentials, we hypothesized that **3** could catalyze the bromination of certain aromatic compounds upon irradiation. In a typical experiment (Figure 3A), 0.20 mM of **3**, 4.0 mM of TMB, and 20 mM of aqueous HBr in 0.750 mL of CD_3CN solution was irradiated by NIR light (LED, λ_{max} = 738 nm, FWHM 34 nm, 370 mW/cm^2). The bromination was monitored by ^{1}H-NMR with dimethylsulfone as an internal standard (Figure 3B). After 30 min irradiation, a brominated product was confirmed. In the NMR spectra, the signal derived from the aromatic ring of TMB at 6.09 ppm shifted to 6.27 ppm, attributed to 2,4,6-trimethoxy bromobenzene (TMB-Br). The absence of new peaks from the other product indicated the high selectivity and conversion yield of the photocatalytic reaction by **3**. The overall reaction yield of the bromination was determined to be >99%.

Notably, no change in the signal intensities of **3** was observed in ^{1}H-NMR spectra after the reaction (Figure S9), confirming its high photo-stability. To determine the longevity of **3**, the reaction was monitored for an extended period using excess TMB and HBr. Figure 3C shows the plot for production over time, fitted with a formula considering the first- or pseudo-first-order kinetics of the formation of TMB-Br and decomposition of **3**. The fitting curve allowed us to estimate the TON of 2830 at a sufficiently long reaction time (t > 500 h), which is, to the best of our knowledge, the highest TON reported for non-metal organic photocatalysts as a single-molecule NIR-photocatalyst (Table S1). This was achieved by the successful molecular design of **3** mentioned above to offering its notable stability. Furthermore, the appropriate photo-oxidation ability of **3** is expected to inhibit undesirable autoxidative degradation, as previously observed with redox reagents that are too strong, such as the Mes-Acr$^+$ system.[32]

The dependency on induced light energy for the reactions was studied by tracking the reaction using various light intensities (Figure 3D). The turnover frequency (TOF) increased with light intensity (1.94, 2.50, and 4.41 min^{-1} for 93, 185, and 370 mW cm^{-2}). This is likely due to the heat generation associated with intense light positively affecting the reaction rate.

Given that the light source used in this study has a peak wavelength of 738 nm and a full-width half maxima (FWHM)of 34 nm (Figure S10), the above reactions were undoubtedly triggered by light above 700 nm. This confirms that **3** is a unique NIR photocatalyst composed of non-metal organic molecules.

Photocatalytic bromination by 3 in the absence of O_2

Surprisingly, **3** could proceed with the photocatalytic bromination without molecular oxygen. This was confirmed through a three-times freezing-thaw process for degassing, followed by the photocatalytic oxidative bromination of TMB with HBr under the NIR illumination (Figure S11). In the absence of O_2, the formation of TMB-Br was observed, whereas a partial decomposition of **3** was observed after the reaction in the absence of O_2 (Figures S11A and S11B). This is likely because O_2 acts as a quencher of an unstable intermediate, most probably the one-electron reduced form of **3** (i.e., **3**$^{\bullet-}$), in the reaction.

The decomposition likely involves the transformation of **3**$^{\bullet-}$ into several possible products. Based on our analysis and literature reports of similar systems,[33–35]we propose that this transformation may occur through dimer formation via radical anion coupling, molecular reduction possibly involving sulfone group cleavage, or intramolecular rearrangement. These pathways align with the known reactivity of sulfone-containing compounds under photochemical conditions. While definitive product identification would require further analyses, this initial framework offers valuable insights into potential decomposition mechanisms of **3**.

In the absence of O_2, substituent quenchers may be Br_2 that presents as a decomposition impurity from HBr, or **3** in its photoexcited state. Although these proceeded with the

photocatalytic reaction, their quenching efficiencies are not as good as O_2, promoting the decomposition of **3** *via* $\mathbf{3}^{\bullet-}$. This result indicated that the photocatalytic reaction of **3** is intrinsically independent of O_2 although it requires an electron acceptor to quench $\mathbf{3}^{\bullet-}$. This reaction mechanism sharply contrasts with previously reported organic NIR-photocatalysts mediated by O_2.[11]

Reaction mechanism of the photocatalytic bromination by 3

The fluorescence lifetimes of **3** with varying concentrations of TMB were measured under conditions mimicking the photocatalytic bromination, that is, in the presence of 20 mM HBr (Figure 4A). As the concentration of TMB increased from 0 to 500 mM, the fluorescence lifetimes decreased from 2.32 ns to <0.6 ns. This suggests a direct electron transfer from TMB to **3** in the singlet excited state, producing a radical cation of TMB and a radical anion of **3**. Notably, argon-purged solutions did not show changes in fluorescence lifetimes, indicating that molecular oxygen does not play a significant role in this stage of electron transfer.

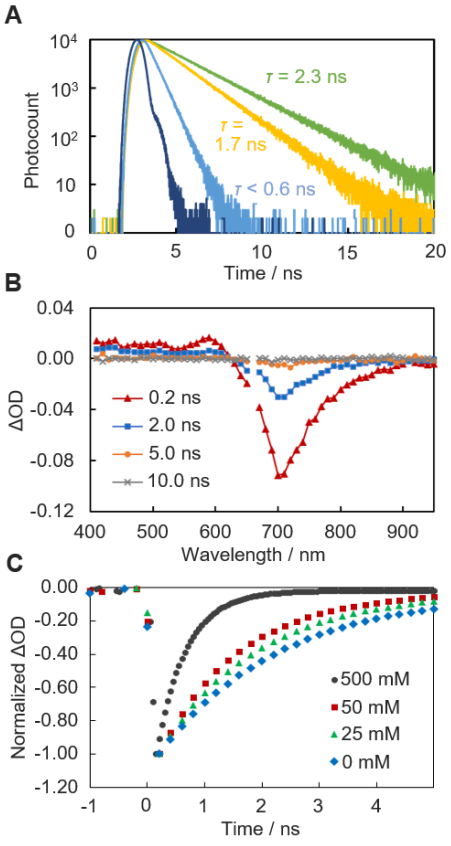

Figure 4. (A) Time-resolved fluorescence decays of **3** in the presence of HBr (WL_{ex}: 630 nm, WL_{em}: 725 nm) with various concentrations of TMB(green: 0 mM, yellow: 50 mM, and blue: 500 mM), and the IRF (dark blue), (B) transient absorption spectra of **3** in the presence of HBr (WL_{ex}: 660 nm), and (C) decay profiles at 640 nm with various concentration of TMB (0, 25, 50 and 500 mM). Solvent: MeCN.

sns-TA spectra of **3** under photocatalytic bromination conditions showed characteristic bands around 500 nm and 700 nm (Figure 4B), similar to those observed for **3** alone (Figure 2A). The key difference was in the rate constants in the presence of TMB (Figure 4C and Figure S12), which increased with increasing TMB concentration, aligning well with the fluorescence lifetime trends (Figure 4A and 4C). The formation of a triplet excited state was ruled out due to the absence of any detectable bands or decay components indicative of such a state.

NTO analysis by DFT calculations predicted the formation of charge-separated states of **3** as meta-stable states (Figure S1B). However, the bands attributed to these charge-separated states were not observed, particularly the characteristic band of the mesityl radical cation around 500 nm,[36] which may originate from the partial structure of **3**. This suggests that the charge-separated state likely has a lifetime shorter than our detection limit (~0.1 ns) in the present condition and may not significantly contribute to electron transfer reactions, given that this lifetime is shorter than the diffusion rate of substrates in MeCN (~0.4 ns).[37] In addition, the sns-TA spectra did not show the detectable signal attributed to $TMB^{\bullet+}$ (450 nm).[27] $TMB^{\bullet+}$ would exhibit a rapid reaction with the excess Br^- promptly forming a Br adduct radical.[27]

These results support a feasible mechanism for the initial stage of the bromination reaction (Scheme 1). The process begins when **3** is excited by NIR light. In its excited state, **3** directly oxidizes aromatic compounds through an electron transfer, producing a radical cation intermediate of the substrate and the reduced form of the catalyst, $\mathbf{3}^{\bullet-}$.

The formed $\mathbf{3}^{\bullet-}$ then transfers an electron to an acceptor in the system. In the present case, as discussed in the previous sub-section, it is predominantly molecular oxygen. $\mathbf{3}^{\bullet-}$ transfers an electron to the surrounding oxygen, generates superoxide (O_2^-), and returns to its ground state.

In acidic conditions of the present reaction, O_2^- can react with protons (H^+) to form hydroperoxyl radical ($HO_2^{\bullet}$) , subtracting hydrogen radical to form hydrogen peroxide (H_2O_2).[27] If O_2 is absent, Br^-, formed due to the electron transfer from $\mathbf{3}^{\bullet-}$ to Br_2, as described above, is expected to take over the role of $HO_2^{\bullet}$. Based on these results, we propose a catalytic reaction scheme as illustrated in Scheme 1. This mechanism highlights the efficient utilization of NIR light by **3** for the bromination.

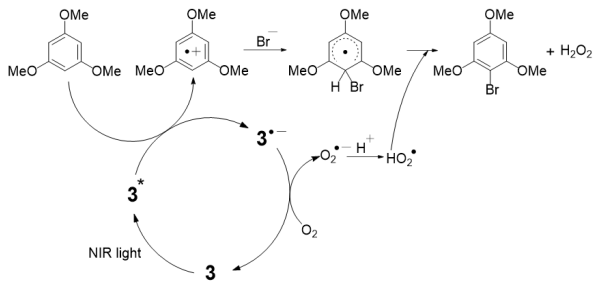

Scheme 1. Proposed catalytic reaction pathway in the presence of O_2

Photocatalytic reaction by 3 for various substrates, including visible light-absorbing molecules

To confirm the versatility of the photocatalytic reaction catalyzed by **3**, we performed photocatalytic brominations of aromatic compounds with different oxidation potentials other than TMB under similar conditions (Figures 5A, S13-16). As shown in Table 2, **3** behaved as the photocatalyst of the bromination for various substrates possessing oxidation potentials lower than +1.33 V, as predicted by the Gibbs energy change for photoinduced electron transfer estimated by eq 1.

Finally, to emphasize the advantages of NIR-photocatalysts and demonstrate the adaptability of **3** for a visible light-absorbing substrate, we conducted a photocatalytic bromination reaction using fluorescein as the substrate (Figure 5B). Fluorescein is a commonly used visible dye that absorbs light below 500 nm (Figure 5C), however it competes for light absorption with most conventional photocatalysts. In a typical experiment, fluorescein (4.0 mM) and **3** (0.20 mM) in a solution of CD_3CN with HBr (600 mM) was mixed. The mixture was irradiated with the LED light source (λ_{max} = 738 nm, FWHM 34 nm, 370 mW/cm^2), forming a red-brownish compound. NMR spectra confirmed the disappearance of the signals of fluorescein in the reaction mixture (Figure S17), and dibrominated fluorescein was confirmed as the product. This result indicated that fluorescein was efficiently brominated. This result highlights the advantage of using NIR light and our NIR photocatalyst **3** for visible light-absorbing substrates.

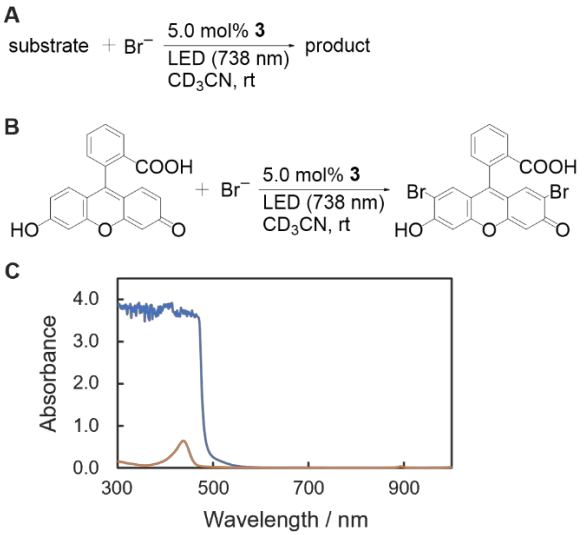

Figure 5. (A) Photocatalytic reaction scheme using **3**, HBr and various substrates shown in Table 2, (B) photocatalytic reaction scheme using **3**, HBr and fluorescein, and (C) absorption spectra of fluorescein of the reaction condition (blue: 4.0 mM) and moderate concentration (orange 15 μM) in MeCN with HBr. The signals over Abs. = 3.5 are saturated signals with noise.

Table 2. Photocatalytic reactions with various substrate

substrate	product	E_{ox1} [V]	E_{ox1} - E_{red1}*	Yield [%][d] (Conv. yield)
			[eV] [c]	
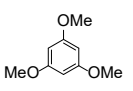	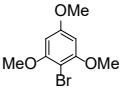	1.05 [a]	-0.28	> 99
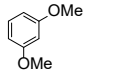	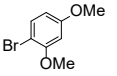	1.11 [a]	-0.24	> 99
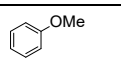	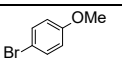	1.38 [a]	+0.03	0
		1.75 [a]	+0.40	0
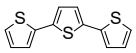	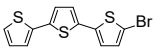	0.59 [a]	-0.76	57 (> 99)
fluorescein	dibrominated[e]	0.87 [b]	-0.48	91 (91)

[a] Obtained from Ref[29], and [b] from Ref[38], where the redox potentials were subtracted by +0.38 to set $Fc^{0/+}$ as the standard. [c] Obtained from eq. 2. [d] Determined by ^{1}H-NMR spectra. [e] The product shown in Figure 5B.

Conclusions

In this study, we have demonstrated the first example of a non-metal NIR organic redox photocatalyst using reductive quenching cycles. It was achieved through the unique properties of aromatic sulfone analogs. Our study highlights several advantages of aromatic sulfones that make them particularly suitable for photoredox catalysis.

1. Low-energy LUMO: This feature affords a low reduction potential as well as a high oxidation potential in the photoexcited state, which is beneficial for photoinduced oxidative reactions.
2. Long-wavelength absorption: The d-orbital on the sulfur atom and π*-bond interaction enables absorption in the NIR region, expanding the usable light spectrum for photocatalysis.
3. High photo-stability: The SO_2 group provides durability against oxidation, which enhances the longevity of the catalyst.

A key finding of our study is that the photocatalytic reaction is essentially independent of molecular oxygen, although oxygen assists in recovering unstable intermediate **3**$^{\bullet-}$. This oxygen independence is practically advantageous because it allows photoredox reactions to be performed at high substrate concentrations without the limitations typically imposed by oxygen solubility.

This study introduces a new class of NIR photocatalysts and provides a versatile approach for designing high-performance organic photocatalysts. The insights gained from this study will pave the way for further developments in the field of photoredox catalysis, potentially leading to applications in areas such as solar energy harvesting, phototherapy, and green chemistry.

ASSOCIATED CONTENT

Data Availability Statement

All experimental data have been provided in the main text and the SI.

Supporting Information.

The Supporting Information is available free of charge at http://pubs.acs.org.

Experimental procedures, Tables of results, additional analyses including UV-Vis and NMR spectra

AUTHOR INFORMATION

Corresponding Author

Vasudevanpillai Biju – Research Institute for Electronic Science,
Hokkaido University,
N20, W10, Kuta-ku, Sapporo, Hokkaido 001-0020, Japan;
Orcid: 0000-0003-3650-9637
Email: biju@es.hokudai.ac.jp
Yuta Takano – Research Institute for Electronic Science,
Hokkaido University,
N20, W10, Kuta-ku, Sapporo, Hokkaido 001-0020, Japan;
Orcid: 0000-0001-9469-6253
Email: tak@es.hokudai.ac.jp

Author Contributions

The manuscript was written through the contributions of all authors. All authors have given approval to the final version of the manuscript. CRediT: Y.T. conceptualized and administrated the project. Y.T. and V.B. supervised and K.Y. investigated and curated the data. K.Y. and Y.T performed the theoretical calculations. T.S. and Y.T performed the transient absorption measurements. K.Y., and Y.T wrote the draft, and all authors edited the manuscript.

Notes

There are no conflicts to declare.

ACKNOWLEDGMENT

We acknowledge financial support from the JSPS KAKENHI (21H01753 and 21K19036 to Y.T.), JST SPRING (JPMJSP2119 to K.Y.), and the JSPS Cooperative Research Program of "NJRC Mater. & Dev." We thank Dr. T. Nakagawa and Dr. T. Kawabata for their technical support on the transient absorption measurements.

REFERENCES

(1) Romero, N. A.; Nicewicz, D. A. Organic Photoredox Catalysis. *Chem. Rev.* **2016**, *116* (17), 10075–10166. https://doi.org/10.1021/acs.chemrev.6b00057.

(2) Adam, W.; Saha-Möller, C. R.; Ganeshpure, P. A. Synthetic Applications of Nonmetal Catalysts for Homogeneous Oxidations. *Chem. Rev.* **2001**, *101* (11), 3499–3548. https://doi.org/10.1021/cr000019k.

(3) Han, C.; Kundu, B. K.; Liang, Y.; Sun, Y. Near-Infrared Light-Driven Photocatalysis with an Emphasis on Two-Photon Excitation: Concepts, Materials, and Applications. *Adv. Mater.* **2024**, *36* (5), 1–25. https://doi.org/10.1002/adma.202307759.

(4) Ravetz, B. D.; Tay, N. E. S.; Joe, C. L.; Sezen-Edmonds, M.; Schmidt, M. A.; Tan, Y.; Janey, J. M.; Eastgate, M. D.; Rovis, T. Development of a Platform for Near-Infrared Photoredox Catalysis. *ACS Cent. Sci.* **2020**, *6* (11), 2053–2059. https://doi.org/10.1021/acscentsci.0c00948.

(5) Wang, C.; Zhang, H.; Zhang, T.; Zou, X.; Wang, H.; Rosenberger, J. E.; Vannam, R.; Trout, W. S.; Grimm, J. B.; Lavis, L. D.; Thorpe, C.; Jia, X.; Li, Z.; Fox, J. M. Enabling In Vivo Photocatalytic Activation of Rapid Bioorthogonal Chemistry by Repurposing Silicon-Rhodamine Fluorophores as Cytocompatible Far-Red Photocatalysts. *J. Am. Chem. Soc.* **2021**, *143* (28), 10793–10803. https://doi.org/10.1021/jacs.1c05547.

(6) Petrone, D. A.; Ye, J.; Lautens, M. Modern Transition-Metal-Catalyzed Carbon–Halogen Bond Formation. *Chem. Rev.* **2016**, *116* (14), 8003–8104. https://doi.org/10.1021/acs.chemrev.6b00089.

(7) Kundu, B. K.; Han, G.; Sun, Y. Derivatized Benzothiazoles as Two-Photon-Absorbing Organic Photosensitizers Active under Near Infrared Light Irradiation. *J. Am. Chem. Soc.* **2023**, *145* (6), 3535–3542. https://doi.org/10.1021/jacs.2c12244.

(8) Han, G.; Li, G.; Huang, J.; Han, C.; Turro, C.; Sun, Y. Two-Photon-Absorbing Ruthenium Complexes Enable near Infrared Light-Driven Photocatalysis. *Nat. Commun.* **2022**, *13* (1), 2288. https://doi.org/10.1038/s41467-022-29981-3.

(9) Sellet, N.; Sebbat, M.; Elhabiri, M.; Cormier, M.; Goddard, J. P. Squaraines as Near-Infrared Photocatalysts for Organic Reactions. *Chem. Commun.* **2022**, *58* (99), 13759–13762. https://doi.org/10.1039/d2cc04707a.

(10) Sellet, N.; Clement-Comoy, L.; Elhabiri, M.; Cormier, M.; Goddard, J. Second Generation of Near-Infrared Cyanine-Based Photocatalysts for Faster Organic Transformations. *Chem. – A Eur. J.* **2023**, *29* (68), e202302353. https://doi.org/10.1002/chem.202302353.

(11) Clark, J. L.; Hill, J. E.; Rettig, I. D.; Beres, J. J.; Ziniuk, R.; Ohulchanskyy, T. Y.; McCormick, T. M.; Detty, M. R. Importance of Singlet Oxygen in Photocatalytic Reactions of 2-Aryl-1,2,3,4-Tetrahydroisoquinolines Using Chalcogenorosamine Photocatalysts. *Organometallics* **2019**, *38* (12), 2431–2442. https://doi.org/10.1021/acs.organomet.9b00126.

(12) M. J. Frisch, G. W. Trucks, H. B. Schlegel, G. E. Scuseria, M. A. Robb, J. R. Cheeseman, G. Scalmani, V. Barone, G. A. Petersson, H. Nakatsuji, X. Li, M. Caricato, A. V. Marenich, J. Bloino, B. G. Janesko, R. Gomperts, B. Mennucci, H. P. Hratchian, J. V., D. J. F. *Gaussian 16, Revision C.01*; Gaussian, Inc., 2016: Wallingford CT.

(13) Krishnan, R.; Binkley, J. S.; Seeger, R.; Pople, J. A. Self-consistent Molecular Orbital Methods. XX. A Basis Set for Correlated Wave Functions. *J. Chem. Phys.* **1980**, *72* (1), 650–654. https://doi.org/10.1063/1.438955.

(14) Petersson, G. A.; Bennett, A.; Tensfeldt, T. G.; Al-Laham, M. A.; Shirley, W. A.; Mantzaris, J. A Complete Basis Set Model Chemistry. I. The Total Energies of Closed-Shell Atoms and Hydrides of the First-Row Elements. *J. Chem. Phys.* **1988**, *89* (4), 2193–2218. https://doi.org/10.1063/1.455064.

(15) Frisch, M. J.; Pople, J. A.; Binkley, J. S. Self-Consistent Molecular Orbital Methods 25. Supplementary Functions for Gaussian Basis Sets. *J. Chem. Phys.* **1984**, *80* (7), 3265–3269. https://doi.org/10.1063/1.447079.

(16) Martin, R. L. Natural Transition Orbitals. *J. Chem. Phys.* **2003**, *118* (11), 4775–4777. https://doi.org/10.1063/1.1558471.

(17) Nakagawa, T.; Okamoto, K.; Hanada, H.; Katoh, R. Probing with Randomly Interleaved Pulse Train Bridges the Gap between Ultrafast Pump-Probe and Nanosecond Flash Photolysis. *Opt. Lett.* **2016**, *41* (7), 1498. https://doi.org/10.1364/OL.41.001498.

(18) Liu, J.; Sun, Y. Q.; Zhang, H.; Shi, H.; Shi, Y.; Guo, W. Sulfone-Rhodamines: A New Class of near-Infrared Fluorescent Dyes for Bioimaging. *ACS Appl. Mater. Interfaces* **2016**, *8* (35), 22953–22962. https://doi.org/10.1021/acsami.6b08338.

(19) Wang, L.; Du, W.; Hu, Z.; Uvdal, K.; Li, L.; Huang, W. Hybrid Rhodamine Fluorophores in the Visible/NIR Region for Biological Imaging. *Angew. Chemie Int. Ed.* **2019**, *58* (40), 14026–14043. https://doi.org/10.1002/anie.201901061.

(20) Grimm, J. B.; Tkachuk, A. N.; Xie, L.; Choi, H.; Mohar, B.; Falco, N.; Schaefer, K.; Patel, R.; Zheng, Q.; Liu, Z.; Lippincott-Schwartz, J.; Brown, T. A.; Lavis, L. D. A General Method to Optimize and Functionalize Red-Shifted Rhodamine Dyes. *Nat. Methods* **2020**, *17* (8), 815–821. https://doi.org/10.1038/s41592-020-0909-6.

(21) Fukazawa, A.; Oshima, H.; Shimizu, S.; Kobayashi, N.; Yamaguchi, S. Dearomatization-Induced Transannular Cyclization: Synthesis of Electron-Accepting Thiophene- S , S -Dioxide-Fused Biphenylene. *J. Am. Chem. Soc.* **2014**, *136* (24), 8738–8745. https://doi.org/10.1021/ja503499n.

(22) Yoshida, K.; Suzuki, T.; Osakada, Y.; Fujitsuka, M.; Miyatake, Y. Exploring Photo-Excited States of Aromatic Sulfones for Efficient NIR-Activated Photothermal Cancer Therapy. *Bull. Chem. Soc. Jpn.* in press.

(23) Epelde-Elezcano, N.; Martínez-Martínez, V.; Peña-Cabrera, E.; Gómez-Durán, C. F. A.; Arbeloa, I. L.; Lacombe, S. Modulation of Singlet Oxygen Generation in Halogenated BODIPY Dyes by Substitution at Their Meso Position: Towards a Solvent-Independent Standard in the Vis Region. *RSC Adv.* **2016**, *6* (48), 41991–41998. https://doi.org/10.1039/C6RA05820E.

(24) Vygranenko, K. V.; Poronik, Y. M.; Wrzosek, A.; Szewczyk, A.; Gryko, D. T. Red Emissive Sulfone-Rhodols as Mitochondrial Imaging Agents. *Chem. Commun.* **2021**, *57* (63), 7782–7785. https://doi.org/10.1039/D1CC02687A.

(25) Xu, S.; Yuan, Y.; Cai, X.; Zhang, C.-J.; Hu, F.; Liang, J.; Zhang, G.; Zhang, D.; Liu, B. Tuning the Singlet-Triplet Energy Gap: A Unique Approach to Efficient Photosensitizers with Aggregation-Induced Emission (AIE) Characteristics. *Chem. Sci.* **2015**, *6* (10), 5824–5830. https://doi.org/10.1039/C5SC01733E.

(26) Takano, Y.; Miyake, K.; Sobhanan, J.; Biju, V.; Tkachenko, N. V.; Imahori, H. Near-Infrared Light Control of Membrane Potential by an Electron Donor–Acceptor Linked Molecule. *Chem. Commun.* **2020**, *56* (83), 12562–12565. https://doi.org/10.1039/D0CC05326K.

(27) Ohkubo, K.; Mizushima, K.; Iwata, R.; Fukuzumi, S. Selective Photocatalytic Aerobic Bromination with Hydrogen Bromide via an Electron-Transfer State of 9-Mesityl-10-Methylacridinium Ion. *Chem. Sci.* **2011**, *2* (4), 715. https://doi.org/10.1039/c0sc00535e.

(28) Hamilton, D. S.; Nicewicz, D. A. Direct Catalytic Anti-Markovnikov Hydroetherification of Alkenols. *J. Am. Chem. Soc.* **2012**, *134* (45), 18577–18580. https://doi.org/10.1021/ja309635w.

(29) Tsudaka, T.; Kotani, H.; Ohkubo, K.; Nakagawa, T.; Tkachenko, N. V.; Lemmetyinen, H.; Fukuzumi, S. Photoinduced Electron Transfer in 9-Substituted 10-Methylacridinium Ions. *Chem. - A Eur. J.* **2017**, *23* (6), 1306–1317. https://doi.org/10.1002/chem.201604527.

(30) Rehm, D.; Weller, A. Kinetics of Fluorescence Quenching by Electron and H-Atom Transfer. *Isr. J. Chem.* **1970**, *8* (2), 259–271. https://doi.org/10.1002/ijch.197000029.

(31) Wilcken, R.; Zimmermann, M. O.; Lange, A.; Joerger, A. C.; Boeckler, F. M. Principles and Applications of Halogen Bonding in Medicinal Chemistry and Chemical Biology. *J. Med. Chem.* **2013**, *56* (4), 1363–1388. https://doi.org/10.1021/jm3012068.

(32) Benniston, A. C.; Elliott, K. J.; Harrington, R. W.; Clegg, W. On the Photochemical Stability of the 9-Mesityl-10-methylacridinium Cation. *European J. Org. Chem.* **2009**, *2009* (2), 253–258. https://doi.org/10.1002/ejoc.200800806.

(33) Oae, S.; Togo, H. Reduction of Sulfonic Acids and Related Organosulfur Compounds with Triphenylphosphine–Iodine System. *Bull. Chem. Soc. Jpn.* **1983**, *56* (12), 3802–3812. https://doi.org/10.1246/bcsj.56.3802.

(34) Angelo, A. C. . D.; Jorge, S. M. A.; Stradiotto, N. R. Electrochemical Evidence of Sulfinic Acid Derivative as an Intermediate in the Reduction of Aromatic Sulfonyl Chloride in an Aprotic Medium. *Eclética Química* **2005**, *30* (3), 57–61. https://doi.org/10.1590/S0100-46702005000300007.

(35) Botrel, A.; Furet, E.; Fourets, O.; Pilard, J.-F. An Experimental and Theoretical Investigation of the Regioselective Cleavage of Aromatic Sulfones. *New J. Chem.* **2000**, *24* (10), 815–820. https://doi.org/10.1039/b001477j.

(36) Fukuzumi, S.; Kotani, H.; Ohkubo, K.; Ogo, S.; Tkachenko, N. V.; Lemmetyinen, H. Electron-Transfer State of 9-Mesityl-10-Methylacridinium Ion with a Much Longer Lifetime and Higher Energy Than That of the Natural Photosynthetic Reaction Center. *J. Am. Chem. Soc.* **2004**, *126* (6), 1600–1601. https://doi.org/10.1021/ja038656q.

(37) Chan, T. C.; Tang, W. K. Diffusion of Aromatic Compounds in Nonaqueous Solvents: A Study of Solute, Solvent, and Temperature Dependences. *J. Chem. Phys.* **2013**, *138* (22). https://doi.org/10.1063/1.4808216.

(38) Shen, T.; Zhao, Z.-G.; Yu, Q.; Xu, H.-J. Photosensitized Reduction of Benzil by Heteroatom-Containing Anthracene Dyes. *J. Photochem. Photobiol. A Chem.* **1989**, *47* (2), 203–212. https://doi.org/10.1016/1010-6030(89)87066-2.

SYNOPSIS TOC (Word Style “SN_Synopsis_TOC”).